Formation of Hydroxyl Radical from the Photolysis of Frozen Hydrogen Peroxide

Liang Chu and Cort Anastasio*

Atmosphere Science Program, Department of Land, Air, and Water Resources, University of California, One Shields Avenue, Davis, California 95616-8627

Received: March 17, 2005; In Final Form: May 16, 2005

Hydrogen peroxide (HOOH) in ice and snow is an important chemical tracer for the oxidative capacities of past atmospheres. However, photolysis in ice and snow will destroy HOOH and form the hydroxyl radical (•OH), which can react with snowpack trace species. Reactions of •OH in snow and ice will affect the composition of both the overlying atmosphere (e.g., by the release of volatile species such as formaldehyde to the boundary layer) and the snow and ice (e.g., by the •OH-mediated destruction of trace organics). To help understand these impacts, we have measured the quantum yield of •OH from the photolysis of HOOH on ice. Our measured quantum yields (Φ(HOOH → •OH)) are independent of ionic strength, pH, and wavelength, but are dependent upon temperature. This temperature dependence for both solution and ice data is best described by the relationship $\ln(\Phi(\text{HOOH} \rightarrow {}^{\bullet}\text{OH})) = -(684 \pm 17)(1/T) + (2.27 \pm 0.064)$ (where errors represent 1 standard error). The corresponding activation energy (E_a) for HOOH (5.7 kJ mol^{-1}) is much smaller than that for nitrate photolysis, indicating that the photochemistry of HOOH is less affected by changes in temperature. Using our measured quantum yields, we calculate that the photolytic lifetimes of HOOH in surface snow grains under midday, summer solstice sunlight are approximately 140 h at representative sites on the Greenland and Antarctic ice sheets. In addition, our calculations reveal that the majority of •OH radicals formed on polar snow grains are from HOOH photolysis, while nitrate photolysis is only a minor contributor. Similarly, HOOH appears to be much more important than nitrate as a photochemical source of •OH on cirrus ice clouds, where reactions of the photochemically formed hydroxyl radical could lead to the release of oxygenated volatile organic compounds to the upper troposphere.

1. Introduction

Atmospheric hydrogen peroxide (HOOH) is both an important oxidant as well as a significant reservoir for the short-lived hydroxyl (•OH) and hydroperoxyl (HO_2•) radicals.[1] This is especially significant, since •OH levels largely determine the oxidizing capacity of the troposphere and thus the lifetimes of many atmospheric trace species.[2] Because of its high solubility, HOOH is a common trace constituent of snow and ice that serves as a relatively stable tracer of the oxidative capacity of past atmospheres.[3,4] Ice core records described by Sigg et al. have shown that HOOH concentrations in snow at Summit, Greenland have increased about 50% over approximately the last 200 years.[5] These records, as well as other studies, have also shown that hydrogen peroxide in snow has a very strong seasonality, with summer concentrations approximately 10 times higher than those in winter, making HOOH a useful tracer for dating snow layers and ice cores.

Results from McConnell et al.[6] indicate that HOOH concentrations in surface snow depend mainly on temperature and atmospheric concentrations of HOOH, while snow grain size also has some effect. Their long-term snowpack simulations indicate that the firn exchanges HOOH with the atmosphere for a decade or more after deposition. The air−snow exchange of HOOH has been further explored by Hutterli and co-workers, who have found that the snowpack can be a strong temperature-dependent source or sink for HOOH.[7] Their work has revealed that this diurnal emission and deposition of HOOH has a large impact on concentrations of HOOH, •OH, and HO_2• in the boundary layer, which in turn affects local atmospheric photochemistry. In addition to this thermal control on the air−snow partitioning of HOOH, there is some preliminary evidence that photochemical reactions on snow grains might also slowly form HOOH in polar snowpacks.[8]

Snowpack hydrogen peroxide is also potentially important as a source of the highly reactive hydroxyl radical. It has already been shown that the photolysis of nitrate, a common trace species in snow and ice, is a source of snowpack •OH and NO_x.[9−12] This photoproduced •OH could affect snowpack and boundary layer chemistry by reacting with organic matter in the snow to form volatile organic compounds, such as formaldehyde, which could be sources of HO_x to the snowpack and overlying atmosphere.[8,13] Oxidation by •OH could also convert snowpack halides into reactive gaseous halogens, which could alter ozone and hydrocarbon chemistry in both the snowpack and the atmosphere.[14] Similarly, the photoformation of •OH from HOOH could affect ice core records of not only HOOH but also trace species that react with •OH such as methane.

While the photolysis of hydrogen peroxide is a known source of •OH in solution,[15−18] its photochemistry on ice has not yet been quantitatively explored. In aqueous solution, ultraviolet radiation splits hydrogen peroxide into •OH with a quantum yield near unity

$$\text{HOOH} + h\nu \rightarrow 2\,{}^{\bullet}\text{OH} \qquad (1)$$

This quantum yield is similar both for tropospherically relevant illumination wavelengths above 290 nm[15] as well as for higher-

* To whom correspondence should be addressed. Phone: (530) 754-6095. Fax: (530) 752-1552. E-mail: canastasio@ucdavis.edu.

10.1021/jp051415f CCC: $30.25
Published on Web 06/29/2005

energy 253.7 nm radiation.[16−18] In addition to this work in aqueous solution, Jacobi and co-workers recently studied the photochemical decomposition of HOOH on ice grains produced in the laboratory using radiation from a 1000 W mercury lamp.[19] They found that HOOH was relatively rapidly destroyed during illumination and suggested that this reaction could be an important sink for hydrogen peroxide as well as a source of hydroxyl radical on polar snow grains.

Our goal in this current work was to quantitatively determine the quantum yields of •OH from HOOH photolysis on ice. These values are needed to understand the impacts of HOOH photolysis as a source of snowpack •OH (and as a sink for HOOH) in the snowpack, in deeper ice, and on atmospheric ice particles. We have determined quantum yields for •OH (i.e., $\Phi(\text{HOOH} \rightarrow {}^{\bullet}\text{OH})$) on illuminated ice pellets as a function of pH, ionic strength, and wavelength. In addition, we have measured the temperature dependence of $\Phi(\text{HOOH} \rightarrow {}^{\bullet}\text{OH})$ for both ice pellets and aqueous solutions.

2. Experimental Methods

2.1. Materials. Hydrogen peroxide, acetonitrile (Optima), sodium borate (certified ACS), sulfuric and perchloric acids (Optima), and potassium hydrogen phthalate were from Fisher. Benzoic acid (99%), sodium benzoate (99%), and horseradish peroxidase were from Aldrich, while *p*-hydroxybenzoic acid (98%) and *p*-hydroxyphenylacetic acid were from TCI America. All chemicals were used as received. Purified water ("Milli-Q") was obtained from a Milli-Q Plus system (≥18.2 MΩ cm).

2.2. •OH and HOOH Measurements. Hydroxyl radicals were measured using a chemical probe technique where photoformed •OH reacts with benzoate/benzoic acid (together referred to as "BA" or "benzoate" for simplicity) to form stable, measurable products that include *p*-hydroxybenzoate (*p*-HBA).[10,20,21] Stock solutions of BA contained 1.4 mM benzoic acid and 12.6 mM sodium benzoate. The BA concentrations used in all sample solutions in this study were high enough to scavenge all photoformed •OH (i.e., [BA]:[HOOH] ≥ 1). We also tried a number of experiments with benzene (instead of benzoate) as a chemical probe for •OH. However, these experiments were unsuccessful, because a significant fraction of the added benzene evaporated from the ice pellet either during sample preparation or subsequent sample handling.

Concentrations of *p*-HBA were measured using an HPLC/UV system described earlier,[20] using calibration standards made in Milli-Q and run during each experiment. HOOH was measured using an HPLC technique with postcolumn derivatization and fluorescence detection.[22] Analyses were performed with a Shimadzu LC-10 AT VP pump and RF-551 fluorescence detector (excitation at 320 nm; emission at 400 nm) using an eluent of 0.1 mM H_2SO_4 and 1 mM Na_2EDTA in Milli-Q at a flow rate of 0.60 mL min^{-1}. Analyses were performed with a 5001-CS guard column and PEEK P#0296−250 × 046 analytical column (MetaChem). Concentrations of HOOH were determined on the basis of calibration standards made in Milli-Q and run during the same day of the experiment.

2.3. Ice Sample Preparation and Illumination. The techniques used for ice pellet preparation and illumination are described fully in Chu and Anastasio[10] and are summarized here. Samples were prepared in a refrigerated chamber by first pipetting 300 μL of Milli-Q water into the well created by a Teflon template placed on a quartz slide backing. After this pure water ice "base" was frozen, the chamber was kept at the experiment temperature (239−268 K), and 100 μL of sample solution was pipetted onto the ice base and allowed to sit until frozen. Sample solutions contained known concentrations of HOOH and benzoate in Milli-Q water (typically 100 μM HOOH and 200 μM BA) and were adjusted to the desired pH using sulfuric acid (pH ≤ 5) or borate (pH ≥ 6). All listed concentrations (e.g., BA and HOOH) and pH values in this paper are for the sample solutions prior to freezing unless specified otherwise.

Ice samples were illuminated for known times using 313 nm (or 334 nm) light from a 1000 W Hg/Xe monochromatic system.[23] Samples were held in a custom-designed (Paige Instruments), Peltier-cooled, temperature-controlled, Teflon-coated copper chamber with a quartz window to transmit light onto the sample. Because of the relatively small photon fluxes in our system, the low concentrations of hydrogen peroxide used, and the short path lengths employed (∼1 mm for the sample solution ice), illumination should have caused only negligible heating of the ice sample.[10] At the end of illumination, the complete ice sample (frozen sample solution and pure water ice base) was melted in the dark at room temperature in about 5−10 min, and then the melted mixture was analyzed for •OH and HOOH as described above.

2.4. Calculation of •OH Quantum Yield. Initial rates of *p*-HBA formation during illumination ($R^*_{p-\text{HBA},\lambda}$) were determined from plots of [*p*-HBA] versus illumination time using a linear regression fit. For each illuminated set of ice samples, rates of *p*-HBA formation were also measured in two controls: (1) in a dark control under identical conditions (sample composition and temperature) except for no illumination (R_{Dark}) and (2) in an illuminated blank control with identical conditions as the sample except that no HOOH was added ($R_{\text{Blank},\lambda}$). The corrected formation rate of *p*-HBA in the illuminated sample was then calculated using $R_{p-\text{HBA},\lambda} = R^*_{p-\text{HBA},\lambda} - R_{\text{Dark}} - R_{\text{Blank},\lambda}$. These blank corrections were small: On average, (±1 σ) R_{Dark} and $R_{\text{Blank},\lambda}$ represented 7 ± 4% and 2 ± 2%, respectively, of the value for $R^*_{p-\text{HBA},\lambda}$. Corrected rates of *p*-HBA formation were converted to rates of •OH formation, $R(\text{HOOH} \rightarrow {}^{\bullet}\text{OH})_\lambda$, by using

$$R(\text{HOOH} \rightarrow {}^{\bullet}\text{OH})_\lambda = R_{p-\text{HBA},\lambda}/Y_{p-\text{HBA}} \qquad (2)$$

where $Y_{p-\text{HBA}}$ is the molar yield of *p*-HBA from the •OH + BA reaction. We determined values of $Y_{p-\text{HBA}}$ using ice pellets made from pH 5.0 solutions containing 10 μM BA, 4 μM HOOH, and Na_2SO_4 to adjust the total ionic strength to between 198 and 628 μM. During 313 nm illumination of the pellets at 263 K, we simultaneously measured the formation rate of *p*-HBA ($R_{p-\text{HBA},\lambda}$) and loss rate of BA ($R_{\text{BA},\lambda}$) and then determined yields of *p*-HBA using $Y_{p-\text{HBA}} = R_{p-\text{HBA},\lambda}/R_{\text{BA},\lambda}$. The average (±$\sigma$) value of $Y_{p-\text{HBA}}$ from these four experiments was 0.083 ± 0.011, which is consistent with the value (0.081 ± 0.014) we determined previously by a somewhat different method.[10] Since this yield is independent of temperature between 243 and 268 K (ref 10), we used $Y_{p-\text{HBA}} = 0.083$ for the temperature-dependence and ionic-strength-dependence experiments with frozen pH 5.0 sample solutions. For the pH-dependence experiments, we used the relationship $Y_{p-\text{HBA}} = -0.0011(\text{pH})^2 + 0.0154(\text{pH}) + 0.0318$ ($R^2 = 0.978$; ref 10). As we reported previously,[10] we also found here that values of $Y_{p-\text{HBA}}$ decrease with decreasing ionic strength, in this case, for ice made from sample solutions with $I < 198$ μM. To avoid the uncertainty introduced by this variation in $Y_{p-\text{HBA}}$, our sample solutions in this work all had ionic strengths of at least 198 μM.

We used 2-nitrobenzaldehyde (2NB) as a chemical actinometer to measure the surface-area-normalized photon flux (I_λ ×

l) in the sample chamber during illumination. The loss of 2NB was measured in ice pellets of the same size and composition as the hydrogen peroxide-containing samples, except that 4 μM 2NB was also added. Under the low light-absorbing conditions of our actinometry, the measured rate constant for 2NB loss ($j_{2NB,\lambda}$) is related to the photon flux through[23]

$$j_{2NB,\lambda} = 2.303 I_\lambda l \epsilon_{2NB,\lambda} \Phi_{2NB,\lambda} \quad (3)$$

where ($\epsilon_{2NB,\lambda}\Phi_{2NB,\lambda}$) is the product of the molar absorptivity and quantum efficiency for 2NB (640 M^{-1} cm^{-1} at 313 nm and 300 M^{-1} cm^{-1} at 334 nm, both at 293 K; ref 23), I_λ is the volume-normalized photon flux (mol−photons L^{-1} s^{-1}), and *l* is the effective path length of the sample (cm). Actinometry performed on ice pellets with and without the chemical components used for the •OH measurements (HOOH, BA, and H_2SO_4) showed that the presence of these chemicals had no effect on measured values of $j_{2NB,\lambda}$. We also found that $j_{2NB,\lambda}$ was independent of temperature in the range 243−268 K, indicating that room-temperature values for the product ($\epsilon_{2NB,\lambda}\Phi_{2NB,\lambda}$) can be used at lower temperatures.[10]

Under our low light-absorbing conditions, the initial rate of •OH formation during illumination of HOOH with radiation of wavelength λ is

$$R(\text{HOOH} \rightarrow {}^\bullet\text{OH})_\lambda = 2.303 I_\lambda\, l\, \epsilon_{\text{HOOH},\lambda} \Phi(\text{HOOH} \rightarrow {}^\bullet\text{OH})_\lambda [\text{HOOH}]_0 \quad (4)$$

where $\epsilon_{HOOH,\lambda}$ is the molar absorptivity of hydrogen peroxide (0.37 M^{-1} cm^{-1} at 313 nm and 274 K; see Table S1 of Supporting Information) and $\Phi(\text{HOOH} \rightarrow {}^\bullet\text{OH})_\lambda$ is the quantum yield of •OH from hydrogen peroxide photolysis. $[HOOH]_0$ is the initial molar concentration of hydrogen peroxide, determined as the HOOH concentration measured after illumination plus the small amount lost during the illumination, that is, $[HOOH]_0 = [HOOH]_{meas} + {}^1/_2 R(\text{HOOH} \rightarrow {}^\bullet\text{OH})_\lambda \times t$, where *t* is the illumination time. We found that it was important to measure HOOH concentrations in the ice pellets, rather than assume the values were the same as those initially delivered in the solution (100 μM), because the pellets often gained or lost a small amount (<10%) of HOOH during experiments. This change in HOOH depended both upon the ionic strength of the sample solution as well as the ice pellet temperature. For ice made from a sample solution with $I = 180$ μM, the ratio of measured [HOOH] to added [HOOH] increased from 1.04 to 1.10 with decreasing temperature between 268 and 239 K, but the correlation was weak ($R^2 = 0.20$). We also tested HOOH in a series of pellets at 263 K made from sample solutions with ionic strengths from 45 μM to 6180 μM. Here, the ratio of measured [HOOH] to added [HOOH] increased from 0.96 to 1.10 over this range of increasing ionic strength ($R^2 = 0.53$). We also tested ice made from pure water (with no added HOOH) and found that, after melting, the samples contained only relatively small amounts of HOOH (<0.5 μM). This indicates that the uptake of HOOH on our ice pellets is not due to contamination during sample preparation. Instead, our results suggest that the sample pellets are exchanging HOOH with the ambient atmosphere. The greater uptake of HOOH at lower temperatures is consistent with the temperature dependence of ice−air partitioning,[24] while the ionic strength dependence likely represents the influence of the thickness of the quasi-liquid layer (QLL). At high ionic strength, the resulting QLL will be thicker and the concentration of HOOH in the QLL relatively low, making it more likely for gas-phase HOOH to dissolve into the QLL. For ice pellets made from low ionic strength solutions, the thin QLL will result in higher concentrations of HOOH; if the concentration is greater than the ice−air partitioning equilibrium value, then a portion of the HOOH will evaporate.

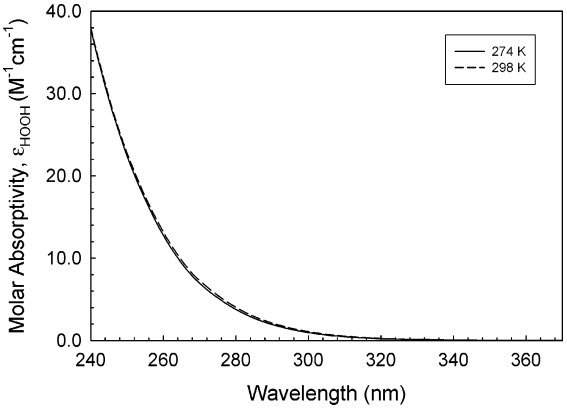

Figure 1. Base-10 molar absorptivities of aqueous hydrogen peroxide at 274 K (solid line) and 298 K (dashed line). Values of $\epsilon_{HOOH,\lambda}$ as a function of temperature and wavelength are tabulated in the Supporting Information (Table S1).

Rearranging eq 3 to solve for I_λ and substituting that into eq 4 produces the expression used to calculate the quantum yield of •OH

$$\Phi(\text{HOOH} \rightarrow {}^\bullet\text{OH})_\lambda = \frac{\epsilon_{2NB,\lambda}\Phi_{2NB,\lambda} R(\text{HOOH} \rightarrow {}^\bullet\text{OH})_\lambda}{j_{2NB,\lambda}\epsilon_{HOOH,\lambda}[\text{HOOH}]_0} \quad (5)$$

Note that we express the quantum yield here as the number of moles of •OH produced per mole of photons absorbed by HOOH, and thus, the maximum value is 2 because of the reaction stoichiometry (eq 1). Thus, the quantum efficiency for HOOH destruction (i.e., the number of moles of HOOH lost per mole of photons absorbed) is one-half the value of $\Phi(\text{HOOH} \rightarrow {}^\bullet\text{OH})_\lambda$.

2.5. Molar Absorptivities of Hydrogen Peroxide as a Function of Temperature. Absorbance spectra of four aqueous HOOH solutions (6.5−26 mM) and a Milli-Q blank were measured in a Shimadzu UV-2501PC spectrophotometer using a stirred 1.0 cm quartz cell and Milli-Q as reference. The sample cell holder was cooled (274−298 K) using chilled water from a recirculating water bath. The molar absorptivity at each wavelength (240−400 nm) was determined as the slope of the linear regression fit to the data of absorbance versus [HOOH].

Our resulting molar absorptivities for aqueous HOOH at 298 K (Figure 1) are very similar to those reported previously.[25] Comparing the 298 K measurements with those made at 274 K (Figure 1) shows that $\epsilon_{HOOH,\lambda}$ changes very little as a function of temperature across the range examined here. In particular, the molar absorptivity of hydrogen peroxide at 313 nm exhibits no significant dependence on temperature, with an average value of 0.386 ± 0.016 M^{-1} cm^{-1} between 274 and 298 K. The best fit values of the molar absorptivities at five temperatures in this range are listed in the Supporting Information (Table S1). Interestingly, although the HOOH molar absorptivities have little temperature dependence, a plot of this relationship (i.e., the slope of $\epsilon_{HOOH,\lambda}$ vs *T*) as a function of wavelength reveals some intriguing structure at wavelengths below 300 nm (Figure S1 of the Supporting Information).

2.6. Measurements of $\Phi(\text{HOOH} \rightarrow {}^\bullet\text{OH})_\lambda$ in Aqueous Solution. Aqueous solutions contained 100 μM HOOH and 200 μM BA and were adjusted to pH 5.0 using sulfuric acid. Samples were illuminated with 313 nm light in stirred, airtight, 1 cm

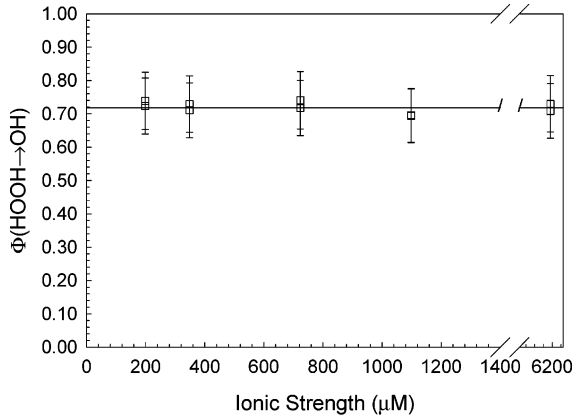

Figure 2. Quantum yields for •OH in ice pellets (263 K; 313 nm illumination) as a function of ionic strength in the sample solution. Each sample solution contained 100 μM HOOH, 200 μM BA, was adjusted to pH 5.0 with H_2SO_4, and contained various amounts of Na_2SO_4 to adjust the ionic strength. Error bars represent ± 1 σ, calculated on the basis of propagated uncertainties in $R_{p-HBA,\lambda}$, I_λ, Y_{p-HBA}, $\epsilon_{HOOH,\lambda}$, [HOOH], and the *p*-HBA calibration curve. The horizontal line is the average value (0.72 ± 0.017).

quartz cells and small aliquots were removed at measured time intervals and analyzed for *p*-HBA. Rates of •OH formation were determined using the same procedure described for the ice pellets (eq 2), except that the value of Y_{p-HBA} in aqueous solution is (0.19 ± 0.01).[10] The quantum yield of •OH was calculated using eq 5, where $j_{2NB,\lambda}$ was the value measured in aqueous 2NB (4 μM) on the same day as the hydrogen peroxide photolysis experiment.

3. Results and Discussion

3.1. Quantum Yield of •OH in Ice as a Function of Ionic Strength. Quantum yields of •OH (Φ(HOOH → •OH)) from hydrogen peroxide photolysis on ice were first measured at 263 K in frozen sample solutions at pH 5.0 that contained 100 μM HOOH, 200 μM BA, and variable amounts of Na_2SO_4 to adjust the ionic strength (*I*). As shown in Figure 2, the plot of Φ(HOOH → •OH) versus *I* has a slope (± 1 standard error) that is not significantly different from zero ($(5.1 \pm 26) \times 10^{-7}$; $p < 0.84$), indicating that the ionic strength of the sample solution has no effect on •OH quantum yields within the range of ionic strengths tested (198−6198 μM). The average value of Φ(HOOH → •OH) in these experiments was 0.72 ± 0.017, which is over 200 times higher than the corresponding value obtained from nitrate photolysis at the same pH and temperature ($(3.4 \pm 0.6) \times 10^{-3}$; ref 10).

3.2. Quantum Yield of •OH on Ice as a Function of pH. To explore the pH dependence of Φ(HOOH → •OH) on ice, we measured values in frozen sample solutions containing 100 μM HOOH and 200 μM BA and with pH values from 2.0 to 7.0. As shown in Figure 3, the •OH quantum yield was essentially constant in these samples, with a slope for the regression line of Φ(HOOH → •OH) versus pH of 0.006 ± 0.004 ($p < 0.93$). The average value (± 1 standard error) for Φ(HOOH → •OH) in these samples was 0.70 ± 0.031, consistent with the value from the ionic strength experiments described above. This absence of a pH effect on Φ(HOOH → •OH) is different from the previously reported case for nitrate, where quantum yields of •OH from NO_3^- photolysis on ice increased from 2.1×10^{-3} at pH 2.0 to 3.6×10^{-3} at pH 7.0 (Figure 3; ref 10). As a check on this pH dependence for nitrate, we remeasured $\Phi(NO_3^- \rightarrow$ •OH) in two sets of ice pellets made from a pH 2.0 sample solution. As shown by the filled circles

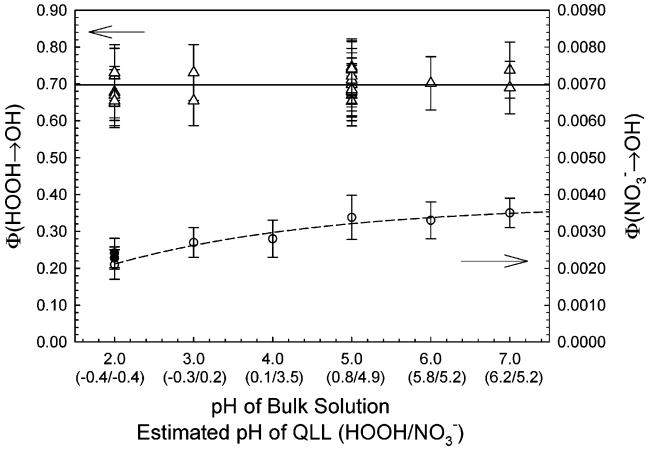

Figure 3. Quantum yields of •OH from HOOH photolysis (open triangles) in ice pellets (263 K, 313 nm illumination) as a function of pH in the sample solution (100 μM HOOH and 200 μM BA). For comparison, the quantum yields of •OH from nitrate photolysis are also plotted: open circles represent data from Chu and Anastasio,[10] while the two closed circles were determined in this present work. Error bars represent ± 1 σ, calculated as described in Figure 2. The pH values listed in parentheses are the estimated values in the quasi-liquid layer of the ice pellets. The solid line through the HOOH data is the average value (0.70 ± 0.031), while the dashed line through the nitrate data is an exponential regression fit.[10]

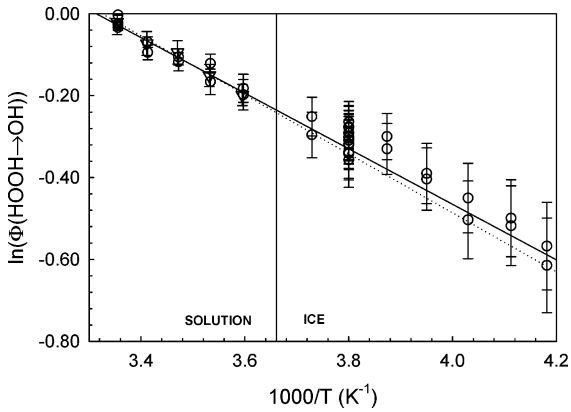

Figure 4. Temperature dependence ($T = 239-318$ K) of Φ(HOOH → •OH) in aqueous and frozen sample solutions containing 100 μM HOOH, 200 μM BA, and adjusted to pH 5.0. The circles are measured data from the present study in both aqueous solution and ice pellets, with errors of $\pm 1\sigma$. The solid line is a linear regression fit to our combined solution and ice data (eq 6). The inverted triangles (with dotted regression line) are solution data from Zellner et al.[15]

in Figure 3, these new measurements are essentially identical to those previously reported. When combined, these results for HOOH and NO_3^- indicate that the pH dependence for •OH formation during nitrate photolysis is real (e.g., it is not an artifact of our BA technique), although its cause is still unexplained.[10]

3.3. Temperature Dependence of •OH Quantum Yields. As the first step in determining the temperature dependence of HOOH photolysis, we measured values of Φ(HOOH → •OH) in aqueous solutions (100 μM HOOH, 200 μM BA, pH 5.0) between 278 and 318 K. As shown in Figure 4, our •OH quantum yields in solution are very similar to those previously reported by Zellner and co-workers [15] and follow the regression $\ln(\Phi(\text{HOOH} \rightarrow \text{•OH})) = -(679 \pm 53)(1/T) + (2.25 \pm 0.016)$ (where errors represent 1 standard error and $n = 12$). The corresponding activation energy ($E_a = 5.6 \pm 0.44$ kJ mol^{-1}) and change in entropy ($\Delta S = 18.7 \pm 0.13$ J mol^{-1} K^{-1}) for our

TABLE 1: Values of E_a and ΔS (± 1 standard error) for the formation of •OH from hydrogen peroxide photolysis in ice and aqueous solution[a]

	E_a (kJ mol^{-1})	ΔS (J mol^{-1} K^{-1})
	Solution Values	
this study	5.6 ± 0.44	18.7 ± 0.13
Zellner et al.[b]	6.0 ± 0.40	19.9 ± 1.3
	Ice Values	
this study	5.8 ± 0.34	19.5 ± 0.83
	Combined Solution and Ice Data	
this study	5.7 ± 0.14	18.9 ± 0.53

[a] The activation energy (E_a) and the change in entropy (ΔS) were calculated on the basis of the linear regression fits to the data of $\ln(\Phi(\text{HOOH} \rightarrow {}^\bullet\text{OH}))$ vs $1/T$: $E_a = -\text{slope} \times R \times 10^{-3}$ (kJ mol^{-1}) and $\Delta S = y\text{-intercept} \times R$ (J mol^{-1} K^{-1}), where R is the gas constant (8.314 J mol^{-1} K^{-1}). [b] Values calculated on the basis of the pH 4−9 data of Zellner et al.[15]

solution data are essentially identical to those previously reported (Table 1).

To complete our temperature dependence study, we also measured quantum yields for •OH in a series of ice pellets ($T = 239-268$ K) prepared from sample solutions identical to those described above. As shown in Figure 4, our values ($\pm 1\sigma$) of $\Phi(\text{HOOH} \rightarrow {}^\bullet\text{OH})$ on ice decreased monotonically with decreasing temperature, ranging from 0.76 ± 0.11 at 268 K to 0.55 ± 0.093 at 239 K. The corresponding regression line for the ice pellet data is $\ln(\Phi(\text{HOOH} \rightarrow {}^\bullet\text{OH})) = -(702 \pm 41)(1/T) + (2.34 \pm 0.10)$ (where errors represent 1 standard error and $n = 27$), which is almost identical to the regression equation for our aqueous solution data described above. Similarly, the activation energy and entropy change calculated from the ice data are statistically indistinguishable from the corresponding values from our aqueous solution data and from those of Zellner and co-workers (Table 1). The fact that our ice pellet and aqueous solution data have the same temperature dependence suggests that the photolysis of hydrogen peroxide on ice between 239 and 268 K in our experiments occurs in a quasi-liquid, or disordered, layer rather than in the bulk ice. This is the same as the case for the photolysis of frozen aqueous nitrate, as described previously.[9,10]

A regression fit to all of our solution and ice data yields the relationship

$$\ln[\Phi(\text{HOOH} \rightarrow {}^\bullet\text{OH})] = -(684 \pm 17)(1/T) + (2.27 \pm 0.064) \quad (6)$$

(where errors represent 1 standard error and $n = 39$), which is very similar to the regressions for the separate ice and aqueous data and which yields similar thermodynamic parameters (Table 1). Given these similarities, we recommend that the regression from the combined data (eq 6) be used to determine •OH quantum yields for both aqueous solutions and ice grains. As shown in Figure 4, this regression line is very similar to that previously reported for aqueous solution. For example, calculated values of $\Phi(\text{HOOH} \rightarrow {}^\bullet\text{OH})$ from our recommended regression (eq 6) at 298 and 239 K are 0.4% lower and 2.7% higher, respectively, compared to values calculated from the extrapolated regression of Zellner et al.[15] Finally, it is interesting to note that the temperature dependence for •OH formation from HOOH photolysis ($E_a = 5.7 \pm 0.14$ kJ mol^{-1}) is much smaller than that from nitrate photolysis ($E_a = 20 \pm 0.89$ kJ mol^{-1}; ref 10). Thus, not only is $\Phi(\text{HOOH} \rightarrow {}^\bullet\text{OH})$ much higher than $\Phi(\text{NO}_3^- \rightarrow {}^\bullet\text{OH})$ in aqueous solution, but this difference is magnified on snow and ice and increases with decreasing temperature.

While the temperature data described above indicate that the photolysis of HOOH occurs in a quasi-liquid layer in our experiments, it should be noted that the distribution of hydrogen peroxide in our ice pellets might be different than that in natural snow. Because we freeze the aqueous hydrogen peroxide solution relatively slowly (over the course of several minutes), essentially all of the solutes in the ice pellet probably reside in quasi-liquid layers at grain boundaries and the air−ice interface. In natural snow, it has been suggested that most snow grain HOOH resides in the bulk ice as a result of co-condensation with water vapor during snow formation,[26] although appreciable amounts (~20%) are also present in the QLL.[27] Although HOOH in bulk ice will still undergo photolysis to produce free •OH, the quantum yield for this process is likely lower than that reported here (eq 6) because of reduced diffusion and enhanced •OH recombination in the ice matrix. These potential differences in distribution are not an issue in the case of frozen nitrate, since NO_3^- is present in the QLL both in natural snow[27] as well as in our previous experiments.[10]

3.4. Wavelength Dependence. We also measured $\Phi(\text{HOOH} \rightarrow {}^\bullet\text{OH})$ during illumination with 334 nm radiation at 263 K to test whether the quantum yield is wavelength dependent. Because of the lower molar absorptivity of hydrogen peroxide at 334 nm (0.083 M^{-1} cm^{-1}; Table S1), we used ice pellets made from sample solutions containing a relatively high hydrogen peroxide concentration (1.0 mM) along with 1.0 mM BA and with a pH of 5.0. The resulting value ($\pm 1\sigma$) of $\Phi(\text{HOOH} \rightarrow {}^\bullet\text{OH})_{334}$ at 263 K was 0.69 ± 0.0082, which is statistically indistinguishable from the average value (0.72 ± 0.017) obtained with 313 nm illumination of the frozen pH 5.0 sample solutions at 263 K. This suggests that the quantum yield of •OH from HOOH photolysis is independent of illumination wavelength throughout at least the UV-A and UV-B portions of the HOOH absorbance tail (i.e., for at least $\lambda > 280$ nm; Figure 1).

4. Environmental Implications.

4.1. •OH Formation in Arctic and Antarctic Snow. Our goal here is to use our measured quantum yields to estimate the relative importance of NO_3^- and HOOH as photochemical sources of •OH in polar snowpacks. The rate of •OH formation from the photolysis of chromophore i on snow grains can be expressed as

$$R(i \rightarrow {}^\bullet\text{OH})_\lambda = 2303/N_A \times I'_\lambda \epsilon_{i,\lambda} \Phi(i \rightarrow \text{OH})_\lambda [i] = j(i \rightarrow {}^\bullet\text{OH})_\lambda [i] \quad (7)$$

$$R(i \rightarrow {}^\bullet\text{OH})_{SUN} = 2303[i]/N_A \times \sum [I'_\lambda \epsilon_{i,\lambda} \Phi(i \rightarrow {}^\bullet\text{OH})_\lambda \Delta\lambda] = \sum [j(i \rightarrow {}^\bullet\text{OH})_\lambda \Delta\lambda][i] \quad (8)$$

where $R(i \rightarrow {}^\bullet\text{OH})_\lambda$ is the rate during illumination with radiation within a given wavelength interval (mol L^{-1} s^{-1} nm^{-1}) and $R(i \rightarrow {}^\bullet\text{OH})_{SUN}$ is the corresponding rate under sunlight illumination (mol L^{-1} s^{-1}). In these equations, I'_λ is the spherically integrated actinic flux (photons cm^{-2} s^{-1} nm^{-1}), $\Delta\lambda$ is the wavelength interval (i.e., the width of the actinic flux interval centered at wavelength λ in units of nm), N_A is Avogadro's number, $\epsilon_{i,\lambda}$ is the base-10 molar absorptivity for chromophore i (e.g., NO_3^- or HOOH, see Table S1 of Supporting Information and ref 10; units of M^{-1} cm^{-1}), $\Phi(i \rightarrow {}^\bullet\text{OH})_\lambda$ is the quantum yield of •OH (eq 6 and ref 10), and $[i]$ is the molar bulk concentration of chromophore in the snow. As shown in the top panel of Figure 5, while both hydrogen

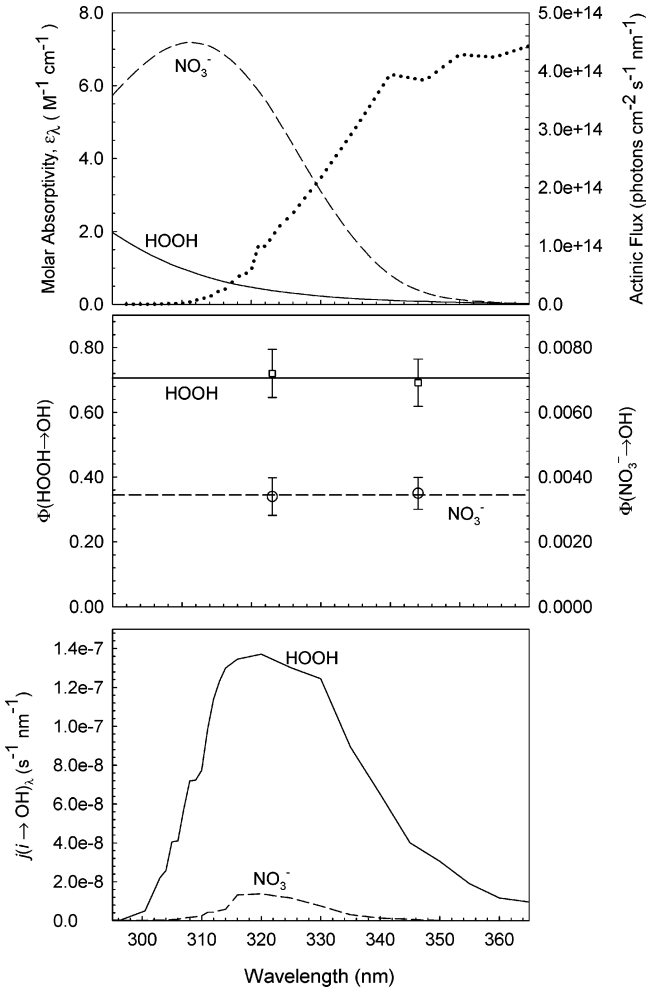

Figure 5. Action spectra for •OH formation from the photolysis of HOOH and NO_3^- on ice. The top panel shows molar absorptivities of aqueous hydrogen peroxide (solid line) and nitrate (dashed line) at 274 K as well as the modeled midday, actinic flux on the summer solstice at Neumayer, Antarctica (70.7 °S, 8.3 °W; dotted line; ref 52). The middle panel shows quantum yields of •OH from the photolysis of HOOH (squares; this work) and nitrate (circles; ref 10) in ice pellets at 263 K. Symbols show data for pellets illuminated with 313 and 334 nm radiation, while the lines represent the recommended quantum yields at 263 K for each chromophore at $\lambda > 290$ nm. The bottom panel shows the wavelength dependence of the rate constants for •OH formation from photolysis of HOOH (solid line) and nitrate (dashed line). The area under each curve is the total rate constant for •OH formation from that chromophore ($j(i \rightarrow$ •OH)) at Neumayer under the conditions described above.

peroxide and nitrate absorb tropospheric UV-A and UV-B radiation, the molar absorptivities for NO_3^- are 7.1 − 2.5 times higher than those of HOOH between 300 and 340 nm, although the HOOH absorption tail extends to longer wavelengths. The situation is reversed, however, with the quantum yields (middle panel of Figure 5): Φ(HOOH → •OH) is 212 times greater than $\Phi(NO_3^- \rightarrow$ •OH) at 263 K, for example. The resulting action spectrum for the rate constants of •OH formation (bottom panel of Figure 5) shows that, for a given concentration, HOOH is a much more effective source of •OH than is nitrate, by a factor of ∼9 for the temperature and actinic flux conditions of Figure 5.

While Figure 5 indicates that the rate constant for •OH formation from HOOH is about an order of magnitude greater than that for •OH from NO_3^- photolysis, comparing the rates of •OH formation from these two chromophores requires that their snowpack concentrations also be taken into account. As shown in Table 2, we have calculated the rate constants ($j(i \rightarrow$ •OH)) and rates ($R(i \rightarrow$ •OH)) of •OH formation on snow grains for four polar locations on days typical for photochemistry experiments at a given site. At all sites, the measured or estimated snow concentrations of HOOH are comparable to, or larger than, the corresponding concentrations of nitrate. In addition, calculated rate constants for •OH formation from HOOH photolysis are 9−22 times greater than those from nitrate, with the greatest differences occurring under conditions with the coldest temperatures. Combining these factors reveals that HOOH is much more important than NO_3^- as a source of snow grain •OH under the conditions examined. Midday rates of •OH formation from hydrogen peroxide photolysis are 11−140 times greater than the corresponding rates from nitrate photolysis, that is, HOOH accounts for 93−99% of the •OH photochemically formed from these two chromophores (Table 2). While the absolute rates of •OH formation from HOOH and NO_3^- at any given location will depend on snow composition, temperature, and actinic flux, our simple overview in Table 2 indicates that hydrogen peroxide is, overall, much more important than nitrate as a source of •OH in both Arctic and Antarctic snowpacks. It should be noted, however, that there could be additional photochemical (or thermal) sources of •OH in snow and that our calculations need to be tested by measurements of •OH in the field.

Table 2 also reveals the approximate photolytic lifetimes of HOOH on polar snow grains. Given that 2 •OH are formed from the photolysis of every HOOH molecule (eq 1), the rate constant for the photochemical destruction of HOOH will be one-half of the rate constant for •OH formation. Thus, midday rate constants for HOOH destruction under the conditions listed in Table 2 range from 0.29×10^{-6} s^{-1} at Alert on the equinox to 2.0×10^{-6} s^{-1} at Summit on the boreal summer solstice. Corresponding lifetimes of HOOH with respect to direct photolysis are 960 h at Alert and 140 h at Summit under these conditions. In addition, our calculated lifetime for photolysis of HOOH on surface snow at Neumayer on the austral summer solstice is 150 h, which is approximately 4 times longer than that estimated by Jacobi et al. from their experiments of snowbound HOOH illuminated with an optically filtered lamp.[19] It should be noted that all of these lifetimes are for midday sunlight conditions and that snow grain HOOH lifetimes in the field will be several times longer as a result of the diurnal changes in actinic flux (except for the South Pole where the diurnal changes in actinic flux are extremely small).

These relatively short photolytic lifetimes of HOOH are in contrast with field measurements, which have shown that hydrogen peroxide concentrations can be preserved both in the near-surface snowpack as well as in deeper ice cores[4,5] These field observations reveal that the net loss of HOOH from snow grains is much smaller than predicted from our photolysis calculations. One possibility for this behavior is that the majority of snow grain HOOH is sequestered in bulk ice where photolysis is likely to be less efficient (section 3.3). However, since photoproducts can migrate out of a water ice cage at temperatures as low as 140 K,[28] even HOOH in the bulk ice of polar snowpacks should undergo photodestruction. An alternate possibility to explain the preservation of HOOH in polar snow and ice is that there is a source of snowpack HOOH of approximately the same magnitude as the photolytic sink. Deposition of atmospheric HOOH appears to be too small to account for this source, given that the amount of HOOH in the boundary layer is much smaller than in the near-surface snowpack and that net deposition fluxes are also relatively small,

TABLE 2: Calculated Rates of Formation of •OH from the Photolysis of Snowpack Hydrogen Peroxide and Nitrate at Sites in the Arctic and Antarctic.

		typical surface snowpack concentration of chromophore i (μM)[c]		rate constant for •OH formation, $j(i \rightarrow {}^{\bullet}OH)_{SUN}$ (10^{-6} s^{-1})[d]		rate of •OH formation, $R(i \rightarrow {}^{\bullet}OH)_{SUN}$ (10^{-12} M s^{-1})		fraction of OH from HOOH
location[a]	date[b]	HOOH	NO_3^-	HOOH	NO_3^-	HOOH	NO_3^-	
Alert, Nunavut	Mar. 21	6	4.2	0.57	0.059	3.5	0.25	0.93
Summit, Greenland	Jun. 21	18	4	4.0	0.26	72	1.0	0.99
South Pole	Dec. 21	10	1.6	1.9	0.088	19	0.14	0.99
Neumayer, Antarctic	Dec. 21	4.8	1.4	3.7	0.42	18	0.59	0.97

[a] Latitudes and longitudes of sampling sites: Alert (82.5 °N, 62.3 °W), Summit (72.6 °N, 38.5 °W), South Pole (90 °S), and Neumayer (70.7 °S, 8.3 °W). [b] Calculations are for midday (solar noon) on the specified date. Temperatures used for calculations at Alert, Summit, South Pole, and Neumayer were 268, 263, 253, and 268 K, respectively. [c] Values are from Anastasio and Jordan[8] (estimated HOOH) and Toom-Sauntry and Barrie[46] for Alert, Hutterli et al.[7] and Dibb et al.[47] for Summit, and Wolff et al.[48] for South Pole. At Neumayer, we used an average of the typical 0−5 mm value of Jacob and Klockow[49] (6.0 μM) and that of Riedel[50] (3.5 μM) for HOOH and the average values of Mulvaney et al.[51] (1.9 μM) and Wolff et al.[48] (0.8 μM) for NO_3^-. [d] The actinic fluxes used in our calculations are from the NCAR TUV model[52] using a wavelength-independent albedo of 0.93 for the snow surface[53] and ozone columns of 306−309 Dobson units.[54] Altitudes used for Alert, Summit, South Pole, and Neumayer were 63, 3200, 2800, and 45 m, respectively.

at least at Summit.[7,29] Instead, we hypothesize that the "missing" source of snowpack HOOH is production within the firn as a result of vigorous HO_x chemistry resulting from abundant levels of precursors such as HCHO and other aldehydes.[29−31] While firn air reactions such as the disproportionation of $HO_2^{\bullet}$ to form HOOH are likely to be significant, the $HO_2^{\bullet}$-mediated formation of HOOH in the quasi-liquid-layers of snow grains is probably also very important, on the basis of the analogous production of HOOH in liquid water cloud drops.[32]

4.2. HOOH Photolysis on Cirrus Ice Clouds. Given its high solubility in ice, especially at lower temperatures,[24] we expect that significant amounts of hydrogen peroxide are present on ice particles in the atmosphere and that this species might play an important role in the chemistry of ice clouds. To explore this issue, we first examine the relative importance of hydrogen peroxide and nitrate as sources of •OH on upper tropospheric cirrus ice clouds under typical conditions (10 km altitude, 238 K, ice water content (L) = 0.1 g m^{-3}, 35 °N, midday, summer solstice). On the basis of an air−ice partitioning coefficient for HOOH at 238 K of 2.4×10^5 mol L^{-1}−ice atm^{-1} (refs 6, 24, 33), and using an equation analogous to the Henry's law gas−aqueous partitioning,[34] we calculate that ~1% of HOOH is present on the cirrus ice particles, while Thibert et al. calculate that 12% of HNO_3 under these conditions will be on the cirrus ice particles.[35] On the basis of typical gas-phase mixing ratios of HOOH and HNO_3 of 500 pptv and 150 pptv, respectively,[36,37] and using the molar absorptivities and quantum yields illustrated in Figure 5, we estimate that the •OH formation rate from HOOH photolysis on ice particles is 7×10^{10} molecules cm^{-3}−ice s^{-1} (equivalent to 7×10^3 molecules cm^{-3}−air s^{-1}), which is ~30 times higher than that from nitrate photolysis. Furthermore, the rate of •OH formation from HOOH photolysis is also greater than the flux of •OH moving from the gas phase to the ice surface, which we calculate to be 3×10^3 molecules cm^{-3}−air s^{-1} based on continuum regime mass transport[34] of gas-phase •OH (1×10^6 molecules cm^{-3}; ref 38) to an ice particle with a diameter of 25 μm (ref 39). Thus, as in polar snowpacks, it appears that HOOH photolysis dominates over nitrate photolysis as an •OH source on cirrus ice particles. It should be noted, however, that this formation of •OH on the ice particles represents <1% of the rate of •OH formation from HOOH photolysis in the gas phase because of the air−ice partitioning of HOOH and the fact that photolysis of gaseous HOOH is somewhat more efficient.[40]

The photolysis of ice-bound HOOH is rapid enough that it might significantly affect gas-phase composition and chemistry. For example, photoformed •OH on the ice could react with organic matter on the particles to possibly form oxygenated volatile organic compounds (OVOCs) which then evaporate to the gas phase. This •OH-mediated release could potentially be a significant source of gaseous oxygenated organics such as formaldehyde, acetaldehyde, acetone, and methanol, which have been found in the upper troposphere at surprisingly high concentrations.[41−43] Analogous •OH-mediated reactions have been proposed for sunlit polar snowpacks, which emit a wide range of OVOCs including aldehydes, ketones, and carboxylic acids.[29−31,44,45] We can estimate an upper-bound rate of this process in cirrus clouds by assuming that every •OH formed on the ice particles reacts with an organic molecule to form an OVOC that then volatilizes to the gas phase. Under this assumption, the rate of release of OVOCs from cirrus ice particles is equal to rate of •OH formation on the ice particles, which is 1×10^4 molecules cm^{-3}−air s^{-1} if we include both the photolysis of ice-bound HOOH (70% of total rate) and the gas-to-particle partitioning of •OH (30% of rate).

To estimate whether this •OH-mediated release from the ice particles is significant, we consider four representative oxygenated organics: formaldehyde, acetaldehyde, acetone, and methanol. As shown in Table 3, if we consider reaction with •OH and direct photolysis as sinks, estimated lifetimes for these compounds in the gas phase range from 6×10^3 s for formaldehyde to 2×10^6 s for methanol. On the basis of typical gas-phase mixing ratios of these species, the corresponding rates of destruction range from 3×10^3 molecules cm^{-3}−air s^{-1} for methanol to 5×10^5 molecules cm^{-3}−air s^{-1} for formaldehyde (Table 3). To determine whether •OH-mediated release from ice particles could be a significant source of any of these OVOCs, we assume that the gaseous oxygenated organics are in approximately steady state and, therefore, that their rates of formation are roughly equal to the calculated rates of destruction shown in Table 3. Comparing these values with our upper-bound estimate for •OH-mediated OVOC release from the ice particles (1×10^4 molecules cm^{-3}−air s^{-1}) indicates that this mechanism is an insignificant source of short-lived species such as formaldehyde ($R_d = 5 \times 10^5$ molecules cm^{-3}−air s^{-1}) but that it could be significant for species with intermediate or relatively long lifetimes (e.g., methanol with $R_d = 3 \times 10^3$ molecules cm^{-3}−air s^{-1}). While there are a number of important uncer-

TABLE 3: Estimated Rates of Loss of Gaseous Oxygenated Organics in the Upper Troposphere (10 km, 238 K, 0.35 atm, 35 °N, midday, summer solstice)

compound (C)	pseudo-first-order rate constant for loss due to •OH, $k_{OH+C}[•OH]$[a] (s^{-1})	photolysis rate constant,[b] j_C (s^{-1})	lifetime,[c] τ_C (s)	rate of loss, R_d (mlc cm^{-3}–air s^{-1})[d]
HCHO	9×10^{-6}	2×10^{-4}	6×10^{3}	5×10^{5}
CH_3CHO	2×10^{-5}	2×10^{-5}	2×10^{4}	3×10^{4}
CH_3COCH_3	1×10^{-3}	3×10^{-6}	3×10^{5}	1×10^{4}
CH_3OH	5×10^{-3}	0	2×10^{6}	3×10^{3}

[a] Calculated using values of the second-order rate constant between compound C and •OH (k_{OH+C}) adjusted to 238 K (ref 40) and an estimated gas-phase •OH concentration of 1×10^6 molecules cm^3–air (ref 38). [b] Photolysis rate constants of the gas-phase oxygenated organics are from the TUV model.[52] [c] Lifetimes of the compounds are calculated as $1/(k_{OH+C}[•OH] + j_C)$. [d] The rate of loss is calculated as $[C]/\tau_C$, where [C] is the gas-phase concentration of C. Estimated values of [C] were 3×10^9, 8×10^8, 5×10^9, and 6×10^9 mlc cm^{-3}–air for HCHO, CH_3CHO, CH_3COCH_3, and CH_3OH, respectively.[42]

tainties in our calculations (e.g., the yield of a particular OVOC from every •OH formed on the ice surface), they do point out that HOOH photolysis on ice particles could affect the gas-phase composition of the upper troposphere. Similarly, the photoformation of condensed-phase •OH likely has even greater effects on the composition (and perhaps properties) of the ice particles themselves.

Acknowledgment. This work was funded by the Office of Polar Programs at the National Science Foundation (OPP-0230288). We thank Ingrid George and Tony Robles for laboratory assistance and the anonymous reviewers.

Supporting Information Available: Base-10 molar absorptivities for aqueous hydrogen peroxide ($\epsilon_{HOOH,\lambda}$) as a function of temperature between 274 K and 298 K at 240 nm to 380 nm are shown in Table S1. Figure S1 shows the temperature dependence of HOOH molar absorptivities as a function of wavelength between 240 nm to 380 nm. This material is available free of charge via the Internet at http://pubs.acs.org.

References and Notes

(1) Finlayson-Pitts, B. J.; Pitts, J. N. *Chemistry of the Upper and Lower Atmosphere: Theory, Experiments, and Applications*; Academic Press: San Diego, 2000.
(2) Thompson, A. *J. Geophys. Res.* **1991**, *96*, 13089.
(3) Kamiyama, K.; Motoyama, H.; Fujii, Y.; Watanabe, O. *Atmos. Environ.* **1996**, *30*, 967.
(4) Neftel, A.; Jacob, P.; Klockow, D. *Nature (London)* **1984**, *311*, 43.
(5) Sigg, A.; Neftel, A. *Nature (London)* **1991**, *351*, 557.
(6) McConnell, J. R.; Bales, R. C.; Stewart, R. W.; Thompson, A. M.; Albert, M. R.; Ramos, R. *J. Geophys. Res.* **1998**, *103*, 10561.
(7) Hutterli, M. A.; McConnell, J. R.; Stewart, R. W.; Jacobi, H. W.; Bales, R. C. *J. Geophys. Res.-Atmos.* **2001**, *106*, 15395.
(8) Anastasio, C.; Jordan, A. *Atmos. Environ.* **2004**, *38*, 1153.
(9) Dubowski, Y.; Colussi, A. J.; Hoffmann, M. R. *J. Phys. Chem. A* **2001**, *105*, 4928.
(10) Chu, L.; Anastasio, C. *J. Phys. Chem. A* **2003**, *107*, 9594.
(11) Honrath, R. E.; Peterson, M. C.; Guo, S.; Dibb, J. E.; Shepson, P. B.; Campbell, B. *Geophys. Res. Lett.* **1999**, *26*, 695.
(12) Honrath, R. E.; Peterson, M. C.; Dziobak, M. P.; Dibb, J. E.; Arsenault, M. A.; Green, S. A. *Geophys. Res. Lett.* **2000**, *27*, 2237.
(13) Dominé, F.; Shepson, P. B. *Science* **2002**, *297*, 1506.
(14) Peterson, M. C.; Honrath, R. E. *Geophys. Res. Lett.* **2001**, *28*, 511.
(15) Zellner, R.; Exner, M.; Herrmann, H. *J. Atmos. Chem.* **1990**, *10*, 411.
(16) Baxendale, J. H.; Wilson, J. A. *Trans. Faraday Soc.* **1956**, *53*, 344.
(17) Hunt, J. P.; Taube, H. *J. Am. Chem. Soc.* **1952**, *74*, 5999.
(18) Volman, D. H.; Chen, J. C. *J. Am. Chem. Soc.* **1959**, *81*, 4141.
(19) Jacobi, H.-W.; Kwakye-Awuah, B.; Schrems, O. *Ann. Glaciol.* in press.
(20) Anastasio, C.; McGregor, K. G. *Atmos. Environ.* **2001**, *35*, 1079.
(21) Zhou, X. L.; Mopper, K. *Mar. Chem.* **1990**, *30*, 71.
(22) Kok, G. L.; McLaren, S. E.; Staffelbach, T. A. *J. Atmos. Ocean. Technol.* **1995**, *12*, 282.
(23) Anastasio, C.; Faust, B. C.; Allen, J. M. *J. Geophys. Res.-Atmos.* **1994**, *99*, 8231.
(24) Conklin, M. H.; Sigg, A.; Neftel, A.; Bales, R. C. *J. Geophys. Res.-Atmos.* **1993**, *98*, 18367.
(25) Morgan, M. S.; van Trieste, P. F.; Garlick, S. M.; Mahon, M. J.; Smith, A. L. *Anal. Chim. Acta* **1988**, *215*, 325.
(26) Sigg, A.; Neftel, A. *J. Atmos. Chem.* **1992**, *14*, 223.
(27) Jacobi, H. W.; Bales, R. C.; Honrath, R. E.; Peterson, M. C.; Dibb, J. E.; Swanson, A. L.; Albert, M. R. *Atmos. Environ.* **2004**, *38*, 1687.
(28) Pursell, C. J.; Conyers, J.; Denison, C. *J. Phys. Chem.* **1996**, *100*, 15450.
(29) Jacobi, H.-W.; Frey, M. M.; Hutterli, M. A.; Bales, R. C.; Schrems, O.; Cullen, N. J.; Steffen, K.; Koehler, C. *Atmos. Environ.* **2002**, *36*, 2619.
(30) Sumner, A. L.; Shepson, P. B.; Grannas, A. M.; Bottenheim, J. W.; Anlauf, K. G.; Worthy, D.; Schroeder, W. H.; Steffen, A.; Dominé, F.; Perrier, S.; Houdier, S. *Atmos. Environ.* **2002**, *36*, 2553.
(31) Boudries, H.; Bottenheim, J. W.; Guimbaud, C.; Grannas, A. M.; Shepson, P. B.; Houdier, S.; Perrier, S.; Dominé, F. *Atmos. Environ.* **2002**, *36*, 2573.
(32) Lelieveld, J.; Crutzen, P. J. *J. Atmos. Chem.* **1991**, *12*, 229.
(33) McConnell, J. R.; Winterle, J. R.; Bales, R. C.; Thompson, A. M.; Stewart, R. W. *Geophys. Res. Lett.* **1997**, *24*, 441.
(34) Seinfeld, J. H.; Pandis, S. N. *Atmospheric Chemistry and Physics: From Air Pollution to Climate Change*; Wiley: New York, 1998.
(35) Thibert, E.; Dominé, F. *J. Phys. Chem. B* **1998**, *102*, 4432.
(36) Lee, M.; Heikes, B. G.; O'Sullivan, D. W. *Atmos. Environ.* **2000**, *34*, 3475.
(37) Chatfield, R. B. *Geophys. Res. Lett.* **1994**, *21*, 2705.
(38) Tan, D.; Faloona, I.; Simpas, J. B.; Brune, W.; Olson, J.; Crawford, J.; Avery, M.; Sachse, G.; Vay, S.; Sandholm, S.; Guan, H.-W.; Vaughn, T.; Mastromarino, J.; Heikes, B.; Snow, J.; Podolske, J.; Singh, H. *J. Geophys. Res.- Atmos.* **2001**, *106*, 32667.
(39) Baumgardner, D.; Chepfer, H.; Raga, G. B.; Kok, G. L. *Geophys. Res. Lett.* **2005**, *32*, L01806; doi: 10.1029/2004GL021300.
(40) Sander, S. P.; Friedl, R. R.; Ravishankara, A. R.; Golden, D. M.; Kolb, C. E.; Kurylo, M. J.; Orkin, V. L.; Huie, R. E.; Molina, M. J.; Moortgat, G. K.; Finlayson-Pitts, B. J. *Chemical Kinetics and Photochemical Data for Use in Atmospheric Studies, Evaluation Number 14*; JPL Publication 02-25: Jet Propulsion Laboratory: Pasadena, CA, 2003.
(41) Crawford, J.; Davis, D.; Olson, J.; Chen, G.; Liu, S.; Gregory, G.; Barrick, J.; Sachse, G.; Sandholm, S.; Heikes, B.; Singh, H.; Blake, D. *J. Geophys. Res.-Atmos.* **1999**, *104*, 16255.
(42) Singh, H. B.; Tabazadeh, A.; Evans, M. J.; Field, D. B.; Jacob, D. J.; Sachse, G.; Crawford, J. H.; Shetter, R.; Brune, W. H. *Geophys. Res. Lett.* **2003**, *30*, 1862; doi: 10.1029/2003GL017933.
(43) Singh, H.; Chen, Y.; Staudt, A.; Jacob, D. J.; Blake, D.; Heikes, B.; Snow, J. *Nature (London)* **2001**, *410*, 1078.
(44) Dibb, J. E.; Arsenault, M. A. *Atmos. Environ.* **2002**, *36*, 2513.
(45) Guimbaud, C.; Grannas, A. M.; Shepson, P. B.; Fuentes, J. D.; Boudries, H.; Bottenheim, J. W.; Dominé, F.; Houdier, S.; Perrier, S.; Biesenthal, T. B.; Splawn, B. G. *Atmos. Environ.* **2002**, *36*, 2743.
(46) Toom-Sauntry, D.; Barrie, L. A. *Atmos. Environ.* **2002**, *36*, 2683.
(47) Dibb, J. E.; Talbot, R. W.; Munger, J. W.; Jacob, D. J.; Fan, S. M. *J. Geophys. Res.-Atmos.* **1998**, *103*, 3475.
(48) Wolff, E. W.; Jones, A. E.; Martin, T. J.; Grenfell, T. C. *Geophys. Res. Lett.* **2002**, *29*, 1944; doi: 10.1029/2002GL015823.
(49) Jacob, P.; Klockow, D.; Fresenius, J. *Anal. Chem.* **1993**, *346*, 429.
(50) Riedel, K. *Reports on polar and marine research 394*; Riemann, F., Wegener, A., Eds.; Institute for Polar and Marine Research, Bremerhaven, Germany, 2001.
(51) Mulvaney, R.; Wagenbach, D.; Wolff, E. W. *J. Geophys. Res.* **1998**, *103*, 11021.
(52) Madronich, S.; Flocke, S. J. The role of solar radiation in atmospheric chemistry. In *Handbook of Environmental Chemistry*; Boule, P., Ed.; Springer-Verlag: Heidelberg, 1998; pp. 1–26. www.acd.ucar.edu/TUV/.
(53) Dickerson, R. R.; Stedman, D. H.; Delany, A. C. *J. Geophys. Res.* **1982**, *87*, 4933.
(54) The_NASA/GSFC_TOMS_Team. Total Ozone Mapping Spectrometer. data http://toms.gsfc.nasa.gov.